NANO EXPRESS

Au Nanoparticles as Interfacial Layer for CdS Quantum Dot-sensitized Solar Cells

**Guang Zhu · Fengfang Su · Tian Lv ·
Likun Pan · Zhuo Sun**

Abstract Quantum dot-sensitized solar cells based on fluorine-doped tin oxide (FTO)/Au/TiO$_2$/CdS photoanode and polysulfide electrolyte are fabricated. Au nanoparticles (NPs) as interfacial layer between FTO and TiO$_2$ layer are dip-coated on FTO surface. The structure, morphology and impedance of the photoanodes and the photovoltaic performance of the cells are investigated. A power conversion efficiency of 1.62% has been obtained for FTO/Au/TiO$_2$/CdS cell, which is about 88% higher than that for FTO/TiO$_2$/CdS cell (0.86%). The easier transport of excited electron and the suppression of charge recombination in the photoanode due to the introduction of Au NP layer should be responsible for the performance enhancement of the cell.

Keywords Quantum dot-sensitized solar cell · Gold nanoparticles · Interfacial layer

Introduction

Quantum dot-sensitized solar cells (QDSSCs) are considered as a promising candidate for the development of next generation solar cells because they can be fabricated by simple and low-cost techniques [1, 2]. The development of nanotechnogy, especially the synthesis and application of nanomaterials [3–8], facilitates the progress of QDSSCs and enables them to receive more and more interests. Currently, the efforts on improving the performance of QDSSCs have mainly been focused on fundamental issues, such as improved understanding of device physics [9], optimization of device structure by advanced processing methods [10, 11] and development of high-performance materials [12–16]. These combined efforts have led to very encouraging power conversion efficiency of 4.22% [17]. However, such efficiency is far away for the practical applications. As a result, further exploration on the optimization of QDSSC performance is necessary.

For QDSSCs, electrons generated by the quantum dots have to pass through numerous grain boundaries and the interfaces between conductive substrate and semiconductor oxide layer to reach the conductive substrate via conduction band of semiconductor oxide. Therefore, the control of the charge carrier transportation at interfaces is one of the most challenging issues in the improvement of QDSSCs. Lee et al. [18, 19] reported the modification of QDSSCs by using single-walled carbon nanotubes (SWCNTs) on indium-doped tin oxide electrodes. The power conversion efficiency of the cell was increased by 50.0% for CdS QDSSCs and 35.6% for PbS QDSSCs due to the improved charge-collecting efficiency and reduced recombination in the presence of SWCNTs. Kim et al. [20] used graphene-TiO$_2$ composite as an interfacial layer between fluorine-doped tin oxide (FTO) layer and nanocrystalline TiO$_2$ for dye-sensitized solar cells. The introduction of graphene-TiO$_2$ increased the efficiency from 4.8 to 5.26% due to the retardation of the back-transport reaction resulting from the direct contact of the electrolyte with the FTO substrate.

As a noble metal, nanosized Au exhibits unusual electric and optical properties as well as high chemical stability [21–23]. Therefore, Au can be considered as an interfacial layer between active layer and conductive substrate to improve the performance of cells. Kouskoussa et al. [24, 25] employed a Au ultrathin layer between FTO or

G. Zhu · F. Su · T. Lv · L. Pan (✉) · Z. Sun
Engineering Research Center for Nanophotonics & Advanced Instrument, Ministry of Education, Department of Physics, East China Normal University, Shanghai, China
e-mail: lkpan@phy.ecnu.edu.cn

aluminum-doped zinc oxide anode and organic electron donor layer to improve the interface resistance of organic solar cells. A higher conversion efficiency of cells had been achieved due to better hole collection efficiency due to the introduction of Au ultrathin layer. However, using nano-sized Au as interfacial layer in the photoanode for improving the QDSSC performance has seldom been reported despite their expected potential to enhance the solar energy conversion efficiency due to favorable charge collection.

In this work, we reported CdS QDSSCs using Au nanoparticles (NPs) as interfacial layer between FTO and TiO$_2$ layer. A large improvement in the efficiency up to 1.62% is achieved when compared with 0.86% for the QDSSC without Au NP interfacial layer. The easier transport of excited electron and the suppression of charge recombination in the photoanode due to the introduction of Au NP layer should be responsible for the performance enhancement of the cell.

Experimental

FTO glass (resistivity: 14 $\Omega/\square$, Nippon Sheet Glass, Japan) was used as the substrate for nanocrystalline TiO$_2$ (P25, Degussa) electrodes. Cadmium nitrate [Cd(NO$_3$)$_2$], sodium sulfide [Na$_2$S], methanol [CH$_3$OH] and ethanol [CH$_3$CH$_2$OH] (analytical grade purity) were purchased from Shanghai Chemical Reagents Co. Ltd. and were used without further purification.

The Au NP colloid solution was prepared by the modified tannic acid/citrate method using chlorauric acid trihydrate, sodium citrate tribasic dehydrate, potassium carbonate anhydrous and tannic acid [26]. The concentration of the Au NPs is about 0.3 mM.

Prior to the fabrication of TiO$_2$ film, FTO glass was ultrasonically cleaned sequentially in HCl, acetone, ethanol and water each for 30 min. After drying in the air, the FTO glass was immersed in Au NP colloid solution at 70°C for 30 min. TiO$_2$ film was prepared by screen printing of TiO$_2$ paste on the FTO glass, followed by sintering at 500°C for 30 min. The thickness of TiO$_2$ layer was about 5 μm.

CdS deposition on the TiO$_2$ film was performed by successive ionic layer adsorption and reaction (SILAR) technique [27]. The film was dipped into an ethanol solution containing 0.33 M Cd(NO$_3$)$_2$ for 30 s, rinsed with ethanol and then dipped for another 30 s into a 0.5 M Na$_2$S methanol solution and rinsed again with methanol. The two-step dipping procedure was considered to be one cycle. It is known that the amount of CdS QDs assembled on the photoanode increases with the number of SILAR cycles. Too thin or too thick CdS layer is not beneficial to the performance of QDSSCs and thus appropriate SILAR cycle

is very important [28, 29]. In our experiments, the best performance of QDSSCs can be achieved for the photoanode assembled with CdS in about 12 SILAR cycles. Direct deposition of CdS on screen-printed TiO$_2$ (TiO$_2$/CdS) film without Au NP interfacial layer by SILAR process with 12 cycles was also carried out for comparison.
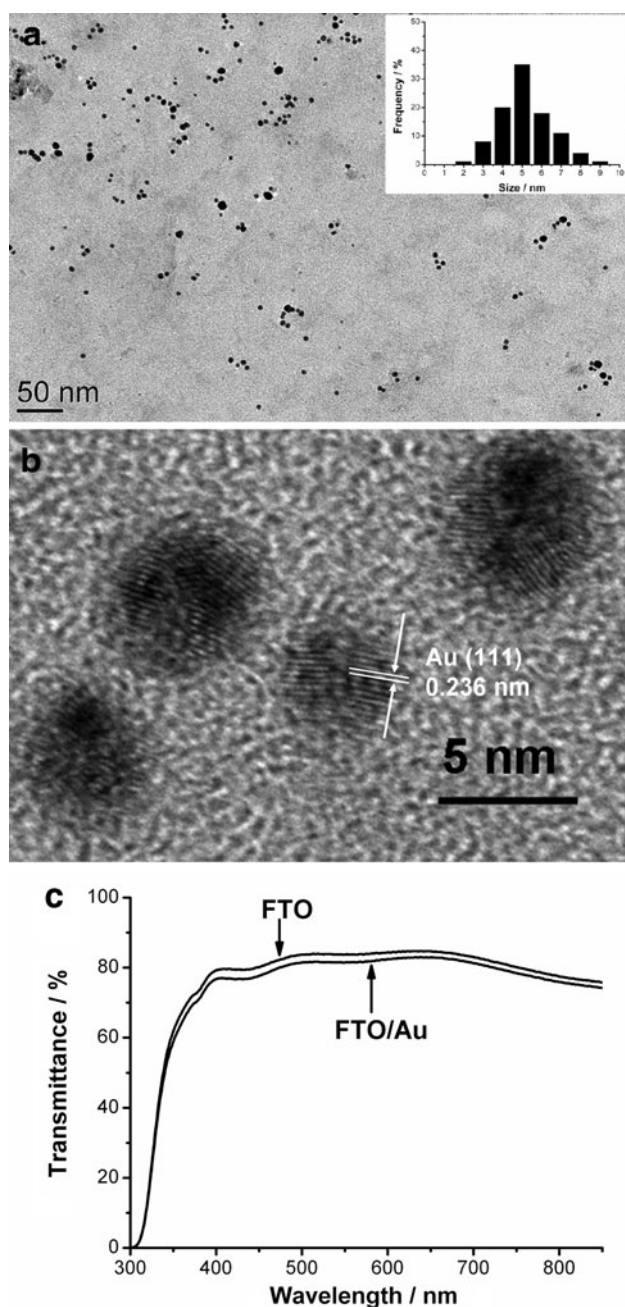
The UV–vis transmittance spectra of FTO glass and FTO glass with Au NPs (FTO/Au) were detected using a UV–vis spectrophotometer (Hitachi U3900). The morphology and structure of TiO$_2$ and TiO$_2$/CdS films were characterized by using a Hitachi S-4800 field emission scanning electron microscopy (FESEM) and a JEOL-2010 high-resolution transmission electron microscope (HRTEM), respectively. Impedance spectroscopy (IS) measurements [30–32] were carried out in dark conditions at forward bias: 0–0.7 V, applying a 10 mV AC sinusoidal signal over the constant applied bias with the frequency ranging between 500 kHz and 0.1 Hz (Autolab, PGSTAT 302 N and FRA2 module).

The QDSSCs were fabricated in a sandwich structure with TiO$_2$ film as photoanode and thin Au-sputtered FTO glass as counter electrode. Water/methanol (3:7 by volume) solution was used as a co-solvent of the polysulfide electrolyte [29]. The electrolyte solution consists of 0.5 M Na$_2$S, 2 M S and 0.2 M KCl. The active area of the cell was 0.25 cm^2. Photocurrent–voltage measurement was performed with a Keithley model 2440 Source Meter and a Newport solar simulator system (equipped with a 1 kW xenon arc lamp, Oriel) at one sun (AM 1.5G, 100 mWcm^{-2}), which was calibrated with a reference Si reference solar cell (P/N 91150 V, Oriel). Incident photon to current conversion efficiency (IPCE) was measured as a function of wavelength from 300 to 800 nm using an Oriel 300 W xenon arc lamp and a lock-in amplifier M 70104 (Oriel) under monochromator illumination, which was calibrated with a mono-crystalline silicon diode.
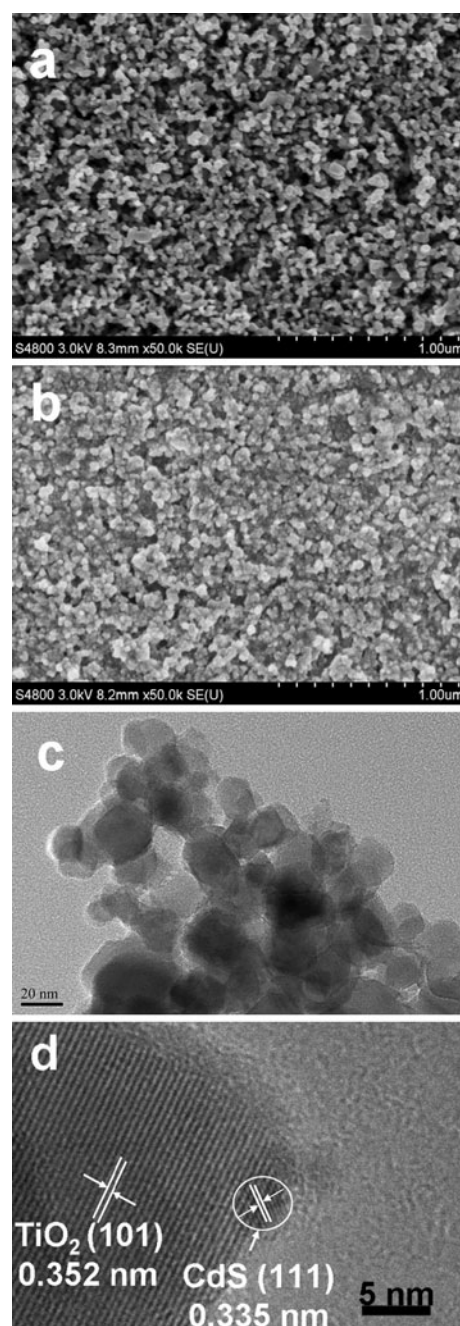
Results and Discussion

Figure 1a shows the low-magnification HRTEM image of Au NPs. The size of Au NPs is mainly distributed from 3 to 8 nm (the inset of Fig. 1a). High-magnification HRTEM image (Fig. 1b) shows that the Au NPs have a d-spacing of 0.236 nm corresponding to (111) lattice plane. The transmittance spectra of FTO and FTO/Au are presented in Fig. 1c. It can be seen that there is little transmittance degradation ($\sim$1%) when FTO is coated with Au NPs, which shall not affect the performance of cells.

Figure 2a and b show FESEM images of TiO$_2$ and TiO$_2$/CdS films, respectively. The TiO$_2$ film is constructed by a random agglomeration of tiny-sized TiO$_2$ nanocrystalline particles. The porous structure of TiO$_2$ favors an easy

Fig. 1 **a** Low-magnification HRTEM image of Au NPs (Inset is the size distribution histogram of Au NPs); **b** high-magnification HRTEM image of Au NPs; **c** transmittance spectra of FTO and FTO/Au

Fig. 2 Surface morphologies of **a** TiO_2 and **b** TiO_2/CdS films by FESEM measurements; **c** Low-magnification and **d** high-magnification HRTEM images of TiO_2/CdS film

penetration of electrolyte, as well as Cd and S precursors, during deposition. When CdS is deposited onto TiO_2 film, an apparent difference in the surface morphology is observed. This result indicates that a great amount of CdS QDs is assembled on the surface of TiO_2 film. Figure 2c shows a low-magnification HRTEM image of TiO_2/CdS film. The larger size of the particles (about 30 nm) when compared with pure P25 TiO_2 particles (about 20–25 nm) indicating the surface of TiO_2 is coated with CdS by

SILAR processes. Figure 2d shows a high-magnification HRTEM image of the interface region in TiO_2/CdS film. The larger crystallite is identified to be a TiO_2 NP. The lattice spacing measured for this crystalline plane is 0.352 nm, corresponding to the (101) plane of anatase TiO_2 (JCPDS 21–1272). Around TiO_2 crystallite edge, fine crystallites are observed. The crystallites connecting to the TiO_2 have lattice fringes of 0.335 nm which is ascribed to (111) plane of CdS (JCPDS 80-0019). Therefore, the

HRTEM image confirms that CdS QDs are attached to the surface of TiO$_2$.

Figure 3 shows the I–V curves of the cells with and without the Au NP interfacial layer (named as FTO/TiO$_2$/CdS and FTO/Au/TiO$_2$/CdS cells). The open circuit potential (V_{oc}), short circuit current (I_{sc}), fill factor (FF) and conversion efficiency (η) of FTO/TiO$_2$/CdS and FTO/Au/TiO$_2$/CdS cells are listed in Table 1. It can be observed that the I_{sc}, V_{oc} and η have increased from 5.72 mAcm^{-2}, 0.47 V and 0.86% for FTO/TiO$_2$/CdS cell to 7.11 mAcm^{-2}, 0.56 V and 1.62% for FTO/Au/TiO$_2$/CdS cell, respectively, while FF increase somewhat. Figure 4 compares the IPCE spectra of FTO/TiO$_2$/CdS and FTO/Au/TiO$_2$/CdS cells. The IPCE is defined as the number of
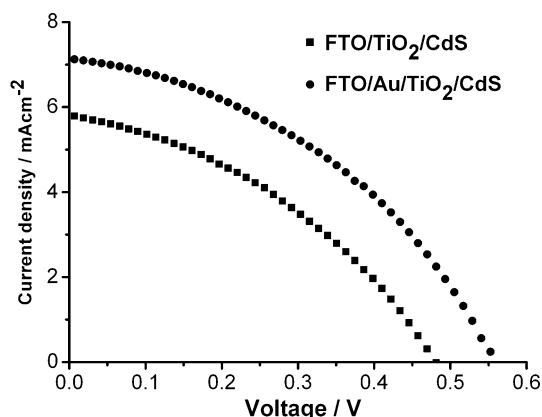
Fig. 3 I-V curves of FTO/TiO$_2$/CdS and FTO/Au/TiO$_2$/CdS cells

Table 1 Photovoltaic parameters of FTO/TiO$_2$/CdS and FTO/Au/TiO$_2$/CdS cells

| Electrode	V_{oc} (V)	I_{sc} (mA/cm^2)	FF	η (%)
FTO/Au/TiO$_2$/CdS	0.56	7.11	0.41	1.62
FTO/TiO$_2$/CdS	0.47	5.72	0.38	0.86
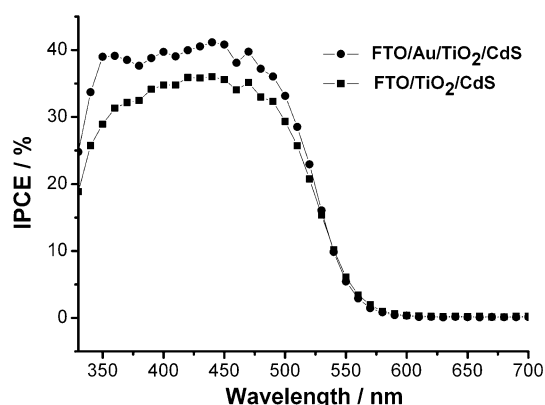
Fig. 4 IPCE curves of FTO/TiO$_2$/CdS and FTO/Au/TiO$_2$/CdS cells

photogenerated charge carriers contributing to the current per incident photon. The FTO/Au/TiO$_2$/CdS cell shows a typical spectral response of TiO$_2$/CdS blend with a maximum IPCE of 41% at 440 nm, while for the FTO/TiO$_2$/CdS cell, the peak reaches 36% only. The insertion of Au NP interfacial layer demonstrates a substantial enhancement of $\sim$14% at 440 nm in the IPCE. This result also indicates that Au NP layer facilitates the excited electron transport from CdS to TiO$_2$ film.

The energy levels of FTO, Au, TiO$_2$ and CdS are schematically shown in Fig. 5a. The conduction band of TiO$_2$ is −4.2 eV (vs. vacuum) [33]. The work function of Au is around −5.1 eV [34], lower than the one of FTO (−4.2–4.4 eV) [35]. However, the contact between Au and FTO can modify the Fermi level of FTO to a lower energy and form a stepwise energy level between TiO$_2$ and FTO/Au. Such a stepwise energy level built in the electrode is advantageous to the electron transfer from TiO$_2$ to FTO via Au NP layer. The easy electron transfer from TiO$_2$ to Au NPs when small-sized Au NPs contact with TiO$_2$ to form a nanoscale heterointerface has also been described by Shibata et al. [36] and Kiyonaga et al. [37]. Figure 5b shows a stepwise structure of energy level for efficient transport of excited electrons in the electrode. The presence of Au NP layer on FTO not only provides efficient electron-transfer route with enhanced charge collection which contributes to the enhanced I_{sc} [38] but also suppresses the charge recombination by reducing back-transport reaction between the electrolyte and FTO substrate which improves the V_{oc} [19]. As a result, the η of the FTO/Au/TiO$_2$/CdS cell is increased remarkably.
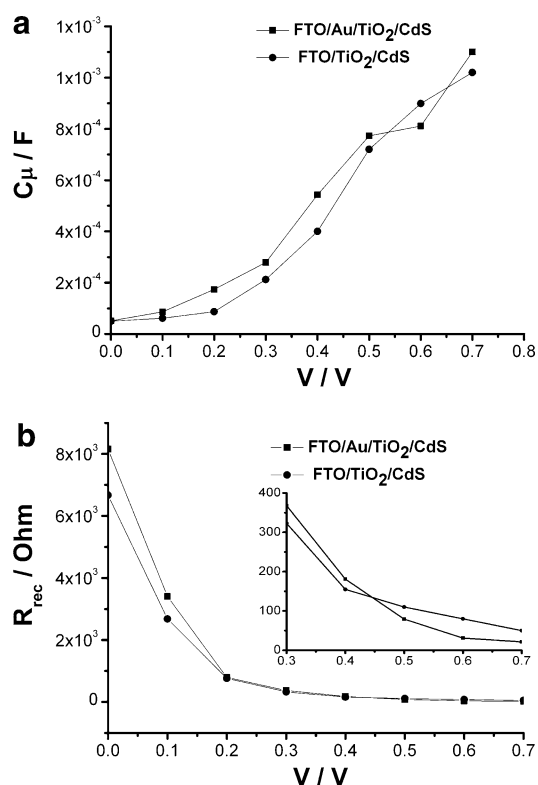
The easier transport of excited electron and the suppression of charge recombination in the photoanode due to the introduction of Au NP layer can be described well by analyzing the impedance data of FTO/TiO$_2$/CdS and FTO/Au/TiO$_2$/CdS cells. The obtained impedance spectra are
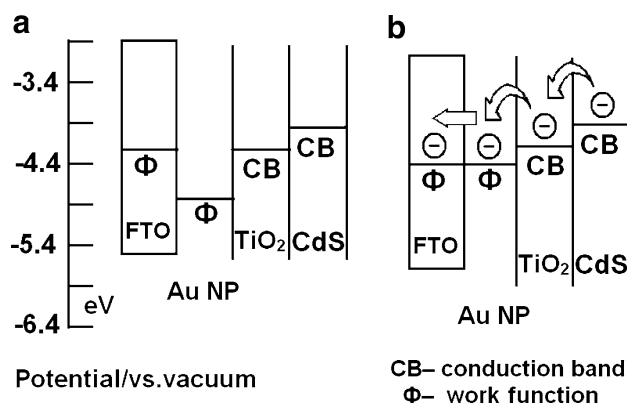
Fig. 5 **a** Schematic diagram of energy levels of FTO, Au, TiO$_2$ and CdS; **b** stepwise structure of energy level for efficient transport of excited electrons in the electrode

characterized by the presence of two semicircles in a Nyquist plot [30, 31]. The high-frequency semicircle is related to the charge transfer at the interfaces of the electrolyte/counter electrode, and the low-frequency one is due to the contribution from the chemical capacitance of nanostructured TiO_2 (C_μ) and the recombination resistance between TiO_2 and the polysulfide electrolyte (R_{rec}) [30, 31]. Figure 6 shows the C_μ and R_{rec} of the cells with and without Au NP layer at various applied potentials obtained from IS fitting. Since the chemical capacitance records the density of states in the TiO_2, the shift of C_μ to lower potential for the cell with Au NP layer indicates a downward displacement of the TiO_2 conduction band (Fig. 6a), which increases the electron injection driving force due to a more favorable QD and TiO_2 conduction band alignment [31]. Figure 6b shows that R_{rec} decreases with the increase in applied potential for both cells. At low potentials, the cell without Au NP layer shows lower recombination resistance (i.e., higher recombination) compared to the cell with Au NP layer, which can explain the higher I_{sc} measured for the cell with Au NP layer [31]. The result further confirms that the introduction of Au NP layer into FTO/TiO_2 electrode favors the electron transport and reduces the charge recombination in the photoanode.

Conclusions

The Au NPs were dip-coated on FTO surface as interfacial layer between FTO and TiO_2 film to improve the photovoltaic performance of QDSSCs. The performance of the cells was investigated. The results show that the η of FTO/Au/TiO_2/CdS cell reaches up to 1.62% under one sun illumination, which is 88% higher than that of FTO/TiO_2/CdS cell. Such an enhancement in photovoltaic performance should be ascribed to the easier transport of excited electron and the suppression of charge recombination in the photoanode due to the introduction of Au NP layer.

Fig. 6 **a** Chemical capacitance (C_μ) and **b** recombination resistance (R_{rec}) as a function of voltage. Inset is the magnified image of (**b**) in a voltage range of 0.3–0.7 V

References

1. B. O'Regan, M. Grätzel, Nature **353**, 737 (1991)
2. W.K. Seok, A.K. Gupta, S.J. Roh, W. Lee, S.H. Han, Bull. Korean Chem. Soc. **28**, 1311 (2007)
3. J. Liu, F. Liu, K. Gao, J.S. Wu, D.F. Xue, J. Mater. Chem. **19**, 6073 (2009)
4. J. Liu, H. Xia, L. Lu, D.F. Xue, J. Mater. Chem. **20**, 1506 (2010)
5. J. Liu, D.F. Xue, Adv. Mater. **20**, 2622 (2008)
6. C.L. Yan, L. Nikolova, A. Dadvand, C. Harnagea, A. Sarkissian, D.F. Perepichka, D.F. Xue, F. Rosei, Adv. Mater. **22**, 1741 (2010)
7. J. Liu, H. Xia, D.F. Xue, L. Lu, J. Am. Chem. Soc. **131**, 12086 (2009)
8. C. Yan, D. Xue, Adv. Mater. **20**, 1055 (2008)
9. P.V. Kamat, J. Phys. Chem. C **112**, 18737 (2008)
10. W.G. Yang, F.R. Wan, S.W. Chen, C.H. Jiang, Nanoscale Res. Lett. **4**, 1486 (2009)
11. U. Ahmad, Nanoscale Res. Lett. **4**, 1004 (2009)
12. S.M. Yang, C.H. Huang, J. Zhai, Z.S. Wang, L. Jiang, J. Mater. Chem. **12**, 1459 (2002)
13. S.C. Lin, Y.L. Lee, C.H. Chang, Y.J. Shen, Y.M. Yang, Appl. Phys. Lett. **90**, 143517 (2007)
14. I. Robel, V. Subramanian, M. Kuno, P.V. Kamat, J. Am. Chem. Soc. **128**, 2385 (2006)
15. R. Plass, P. Serge, J. Kruäger, M. Grätzel, J. Phys. Chem. B **106**, 7578 (2002)
16. P. Hoyer, R. Koänenkamp, Appl. Phys. Lett. **66**, 349 (1995)
17. Y.L. Lee, Y.S. Lo, Adv. Funct. Mater. **19**, 604 (2009)
18. W. Lee, J. Lee, S. Lee, W. Yi, S.H. Han, B.W. Cho, Appl. Phys. Lett. **92**, 153510 (2008)
19. W. Lee, J. Lee, S.K. Min, T. Park, W. Yi, S.H. Han, Mater. Sci. Eng. B **156**, 48 (2009)
20. S.R. Kim, M.K. Parvez, M. Chhowalla, Chem. Phys. Lett. **483**, 124 (2009)
21. C.B. Murry, C.R. Kagan, M.G. Bawendi, Science **270**, 1335 (1995)
22. B.F. Ziolo, E.P. Giannelis, B.A. Weinstein, M.P. O'Horo, B.N. Ganguly, V. Mehrotra, M.W. Russell, D.R. Huffmann, Science **257**, 219 (1992)

23. C.P. Collier, R.J. Saykally, J.J. Shiang, S. Henrichs, Science **277**, 1978 (1997)
24. B. Kouskoussa, M. Morsli, K. Benchouk, G. Louarn, L. Cattin, A. Khelil, J.C. Bernede, Phys. Status Solidi A **206**, 311 (2009)
25. J.C. Berned, Y. Berredjem, L. Cattin, M. Morsli, Appl. Phys. Lett. **92**, 083304 (2008)
26. J.W. Slot, H.J. Geuze, Eur. J. Cell Biol. **38**, 87 (1985)
27. D.R. Baker, P.V. Kamat, Adv. Funct. Mater. **19**, 805 (2009)
28. Y.J. Tak, S.J. Hong, J.S. Lee, K.J. Yong, J. Mater. Chem. **19**, 5945 (2009)
29. Y.L. Lee, C.H. Chang, J. Power Sources **185**, 584 (2008)
30. I. Mora-Sero, S. Gimenez, F. Fabregat-Santiago, R. Gomez, Q. Shen, T. Toyoda, J. Bisquert, Acc. Chem. Res. **42**, 1848 (2009)
31. E.M. Barea, M. Shalom, S. Gimenez, I. Hod, I. Mora-Sero, A. Zaban, J. Bisquert, J. Am. Chem. Soc. **132**, 6834 (2010)
32. G.P. Smestad, F.C. Krebs, C.M. Lampert, C.G. Granqvist, K.L. Chopra, X. Mathew, H. Takakura, Sol. Energy Mater. Sol. Cells **87**, 117 (2005)
33. M. Grätzel, Nature **414**, 338 (2001)
34. B. Kouskoussa, M. Morsli, K. Benchouk, G. Louarn, L. Cattin, A. Khelil, J.C. Bernede, Phys. Status Solidi A **206**, 311 (2009)
35. A.C. Arias, L.S. Roman, T. Kugler, R. Toniolo, M.S. Meruvia, I.A. Hummelgen, Thin Solid Films **371**, 201 (2000)
36. N. Shibata, A. Goto, K. Matsunaga, T. Mizoguchi, S.D. Findlay, T. Yamamoto, Y. Ikuhara, Phys. Rev. Lett. **102**, 136105 (2009)
37. T. Kiyonaga, M. Fujii, T. Akita, H. Kobayashi, H. Tada, Phys. Chem. Chem. Phys. **10**, 6553 (2008)
38. S.H. Kang, J.Y. Kim, Y. Kim, H.S. Kim, Y.E. Sung, J. Phys. Chem. C **111**, 9614 (2007)